Available online at www.sciencedirect.com
SCIENCE DIRECT
Journal of Sound and Vibration 296 (2006) 195–208
JOURNAL OF SOUND AND VIBRATION
www.elsevier.com/locate/jsvi

An investigation into active vibration isolation based on predictive control Part I: Energy source control

H.Z. Fei[a,*,1], G.T. Zheng[b,2], Z.G. Liu[a]

[a]School of Power and Energy Engineering, Harbin Engineering University, Harbin 150001, PR China
[b]School of Astronautics and Aeronautics, Tsinghua University, Beijing 100084, PR China

Received 8 November 2004; received in revised form 11 January 2006; accepted 21 February 2006
Available online 23 May 2006

Abstract

We report the results of a recent study for the active vibration isolation with whole-spacecraft vibration isolation as an application background into which three parts are divided: (i) energy source control, (ii) nonlinearity and time delay, (iii) implementation and experiment. This paper is the first in this three-part series report, which presents theoretical and experimental investigations into pressure tracking system for energy source control of the isolator.

Considering the special environment of the rocket and expected characteristics of actuators, where the isolator will be arranged between the rocket and the spacecraft, pneumatic actuator is proposed to realize the active isolation control. In order to improve the dynamic characteristics of the pneumatic isolator, a cascade control algorithm with double loop structure and predictive control algorithm for pressure tracking control of the inner loop are proposed.

In the current paper, a pressure tracking control system using model predictive control (MPC) is studied first. A pneumatic model around pressure work point is built firstly by simplifying the flow equation of valve's orifices and pressure differential equation of the chambers. With this model, an MPC algorithm in the state space is developed, and problems including control parameter choice and command horizon generator are discussed in detail. In addition, by adding model error correction loop and velocity compensation feedback, effects of model uncertainty and volume variation of chambers are reduced greatly. Thus with this design, the real-time pressure tracking can be guaranteed, and so that the active control system can work at higher frequency range.

1. Introduction

A satellite has to be designed to survive its launch environment since this is the worst-case loading condition for it. This results in an over design of the satellite structure and hence an increment of the launch cost. A lot of effort has been devoted to investigating an approach to improving the launch environment since 1993 [1–6],

*Corresponding author. Tel./fax: +86 451 82568316.
E-mail addresses: feihz@hit.edu.cn (H.Z. Fei), yongqingtu@263.net (G.T. Zheng), liuzhigang@hrbeu.edu.cn (Z.G. Liu).
[1]Former PhD student of Harbin Institute of Technology, Harbin, China.
[2]Also worked with Harbin Institute of Technology, Harbin, China.

0022-460X/$ - see front matter © 2006 Elsevier Ltd. All rights reserved.
doi:10.1016/j.jsv.2006.02.021

which is inserting an isolation system between the launch vehicle and the satellite to reduce the launch-induced vibration of a satellite.

Payloads (e.g., satellites) are attached to launch vehicles by structural adapters known as payload adapter fittings (PAF). Generally, the PAFs are substantially rigid, thereby vibration from the launch vehicle is transmitted without dissipation directly to the payloads. Whole-spacecraft isolation is realized by designing an isolation system substituting the original rigid structure so that vibration transmitted to the payloads can be decreased. To date, at least two types of whole-spacecraft isolation systems have been designed. One is to insert isolation components into PAFs structure, which include uniaxial and multiaxis damped flexure element. One merit of this approach is that it does not need to change the primary configuration of the PAFs [4]. This type of isolation system has successfully flown for many times [3–5]. The other is to replace the PAF structure with an isolation platform [6–8]. In literature [6,7], an isolation platform consisting of eight struts is demonstrated. In this structure each strut is a single passive hydraulic isolator, and every two struts are connected by a unique cross-link, which could induce high stiffness in the lateral direction. In addition, a three-degrees-of-freedom isolation system with a mechanical constraint for whole-spacecraft isolation application is studied in literature [8].

Presently, the whole-spacecraft isolation technique applied in launches is only limited to the passive isolation, and active isolation methods are still under research in labs. Adding active isolation based on passive isolation could improve the performance of whole-spacecraft isolation and realize automatic regulation of the isolation system. In our research project, a kind of isolation platform with eight struts for the whole-spacecraft vibration isolation is being investigated. This system integrates passive and active isolation function together. As a part of the whole project, active control technique with single isolator is investigated in detail in this series report.

This article is the first part, which presents the research on the pressure tracking control system based on model predictive control (MPC). To ensure that the active control system can work effectively in a wide and high frequency range, as the energy supply, the response of air pressure control should be sufficient fast and of high quality. Effort devoted to reaching this target is discussed in detail in this part of the report. The present paper is divided into five parts, and they are: introduction, actuator definition, control strategy investigation, pressure tracking control design and experiment study.

2. Actuator definition

2.1. Actuator choice

The actuator design is a crucial problem in isolation system. The choice of actuator and its driving energy device suffers restrictions from launch vehicle, such as energy source, size and mass, and has to satisfy requirements of spacecraft manufacturers, such as higher reliability, safety and without contamination.

Actuators applied to a large isolation platform usually include piezoelectric, hydraulic, pneumatic and voice coil [9]. Piezoelectric actuators require very high voltage direct current as driving energy, which is difficult to realize in the current launch vehicles. The energy density of voice coils is too low to meet the requirement of whole-spacecraft isolation. And hydraulic actuators could supply large force, but the possible oil leakage would pollute the spacecraft. With such merits as high reliability, without pollution and relative lager actuation stroke and force, pneumatic actuators are attractive to be used for realizing the active control. Another benefit of using pneumatic actuator is that the energy can be supplied by the existing air supply system of a launch vehicle, thus the cost and weight can be significantly reduced. In this paper, pneumatic actuators are chosen as the actuators of the isolation platform.

2.2. Actuator structure

The actuator is designed to integrate active and passive isolation function together and its structure is showed in Fig. 1. There are four chambers in the actuator, the two upper chambers are filled with oil that forms passive damping, and the other two low chambers are filled with air that can produce active control force. Damping value can be changed by adjusting orifices connecting with two upper chambers. Two

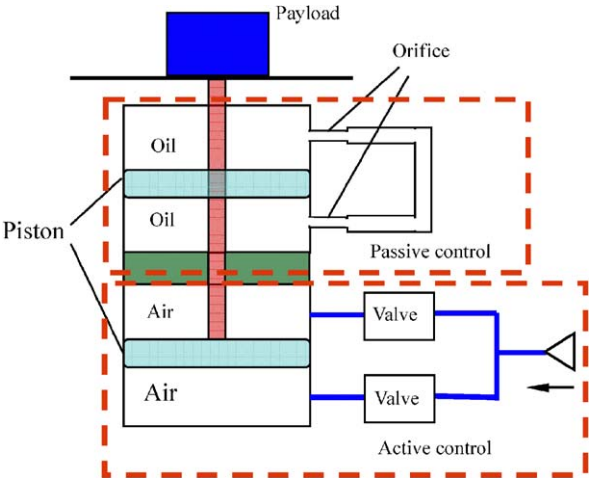

Fig. 1. Structure of the actuator.

proportional directional valves control the pressures of the two low chambers, respectively. Fig. 2 is the photo of the actuator.

2.3. Characteristics of pneumatic spring

Double chambers structure with air is equivalent to a pneumatic spring. The stiffness value of the pneumatic spring is important to the isolation system.

At a constant temperature, relation of absolute pressure and volume in the chamber is

$$PV^n = \text{constant}, \tag{1}$$

where n is thermal coefficient. When moving the piston opposite to the initial position of distance s, the pressure of upper chamber and low chamber are, respectively:

$$P_u = P_{u0}\left(\frac{l_{u0}}{l_{u0}+s}\right)^n, \quad P_d = P_{d0}\left(\frac{l_{d0}}{l_{d0}-s}\right)^n, \tag{2}$$

where l_{u0}, P_{u0} are the length and pressure of the upper chamber at an initial state and l_{d0}, P_{d0} the length and pressure of the low chamber at an initial state. Then the relationship of load force F and stroke s can be written as

$$F = P_d A_d - P_u A_u = p_{d0} A_d \left(\frac{l_{d0}}{l_{d0}-s}\right)^n - p_{u0} A_u \left(\frac{l_{u0}}{l_{u0}+s}\right)^n, \tag{3}$$

where A_u and A_d are the area of upper and down chamber, respectively. Then the stiffness of the pneumatic spring is derived from Eq. (3) as

$$\begin{aligned} k = \frac{\mathrm{d}F}{\mathrm{d}s} &= P_{d0}A_d n\left(\frac{l_{d0}}{l_{d0}-s}\right)^{n-1}\frac{l_{d0}}{(l_{d0}-s)^2} + P_{u0}A_u n\left(\frac{l_{u0}}{l_{u0}+s}\right)^{n-1}\frac{l_{u0}}{(l_{u0}+s)^2} \\ &= \frac{P_{d0}A_d n}{l_{d0}-s}\left(\frac{l_{d0}}{l_{d0}-s}\right)^n + \frac{P_{u0}A_u n}{l_{u0}+s}\left(\frac{l_{u0}}{l_{u0}+s}\right)^n = \frac{P_d A_d n}{l_d} + \frac{P_u A_u n}{l_u}, \end{aligned} \tag{4}$$

where $l_d = l_{d0} - s$ and $l_u = l_{u0} + s$.

It can be seen from Eq. (4) that there exists a nonlinear relation between stiffness and stroke of the pneumatic spring. Fig. 3 plots the curve of stiffness versus stroke when the initial position of the piston is set in the middle of the cylinder. As shown in the figure, stiffness of the pneumatic spring at $s = 4$ mm is 1.17 times of the value when the piston is at the initial position. Since the active isolation is realized by adjusting piston slightly based on the passive isolation, changes in the pneumatic spring stiffness would be very small during

Fig. 2. Photo of the actuator.

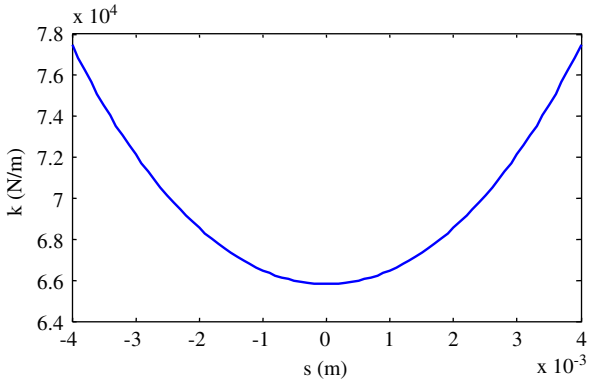

Fig. 3. Curve of stiffness versus stroke.

the active control procedure. So the passive stiffness in the dynamics equation of isolation system is assumed invariable. This assumption will be used in part III of this series report.

3. Control strategy investigation

Although applying pneumatic control to whole-spacecraft isolation has many benefits, due to the air compressibility, the bandwidth of pneumatic servo system generally is too narrow to meet the requirement of active control. A cascade control system with double close loop structure is proposed here for the active isolation system that is showed in Fig. 4. In this control structure, there are two close loops, the inner loop is pressure control system and the outer loop is isolation control system. By adding inner loop specialized for the pressure control, the control system can suppress the disturbance quickly and improve the effectively dynamic

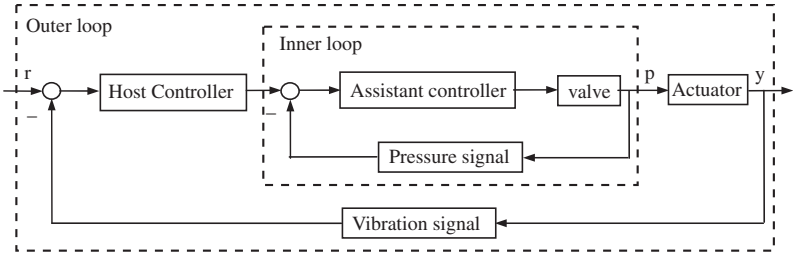

Fig. 4. Structure of cascade isolation system.

characteristics of pressure tracking. Most importantly, the real-time pressure tracking can be guaranteed, and thus the active control system can still work well at a higher frequency range.

In the inner loop, the pressure tracking system exhibits stronger nonlinearity and has time-delay. These add difficulties to modeling and controller design. To effectively overcome these difficulties, in this paper, MPC based on the state space description is proposed for the pressure controller design. MPC exhibits a series of advantages over other methods, such as multiple step prediction and feedback correction, and is suited for complex process control including systems with long delay times or nonlinearity [10]. In fact, MPC is a kind of computer control algorithm. At each sampling instant, using the current state of the plant as the initial state, a finite horizon open-loop optimal control problem is solved, and the optimization yields an optimal control sequence in which the first one is applied to the plant. Another advantage of the MPC controller over other tracking controllers is that it can act in advance of the actual time when there is a change in the setpoint. These characteristics of MPC make it easy to design a controller for the plant of nonlinearity and delay times.

In the outer loop, rate feedback is applied for active isolation control.

4. Pressure tracking control design

Inner loop is an important part of the whole active isolation control system and will affect the performance of the isolation control system greatly. Therefore, it is necessary to specifically study the inner loop of pressure tracking control.

4.1. Modeling

Valves are important components in pneumatic system. In experiment, a 3-stage 5-port valve is used. It has two load ports, i.e. it can control two chambers' pressure simultaneously. To control the pressure of two chambers independently, two valves are used. Gas flow equivalent chart of the valves is showed in Fig. 5 in which arrows denote the flow directions of air.

There are four orifices in each valve, but only two of them are used in the experiment system. The quality flow equation of each chamber includes charging and discharging procedure of the valve. The quality flow of upper chamber q_u and low chamber q_d can be expressed by the following equations:

$$q_u = \psi_{u1}(p_u, p_s)A_{u1} - \psi_{u2}(p_u)A_{u2}, \tag{5}$$

$$q_d = \psi_{d1}(p_d, p_s)A_{d1} - \psi_{d2}(p_d)A_{d2}. \tag{6}$$

In the above equations,

$$\psi_{u1}(p_u, p_s) = p_s(RT_s)^{-1/2}c(1-\sigma_*)^{1/2}\varphi(p_u/p_s, \sigma_*), \tag{7}$$

$$\psi_{u2}(p) = p_u(RT_u)^{-1/2}c(1-\sigma_*)^{1/2}\varphi(p_a/p_u, \sigma_*), \tag{8}$$

$$\psi_{d1}(p_d, p_s) = p_s(RT_s)^{-1/2}c(1-\sigma_*)^{1/2}\varphi(p_d/p_s, \sigma_*), \tag{9}$$

$$\psi_{d2}(p_d) = p_d(RT_d)^{-1/2}c(1-\sigma_*)^{1/2}\varphi(p_a/p_d, \sigma_*), \tag{10}$$

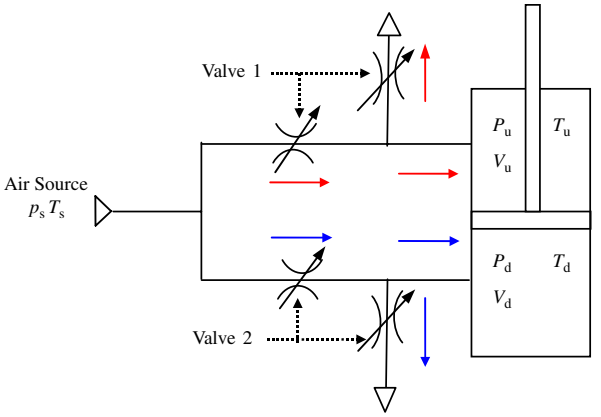

Fig. 5. Gas flow equivalent chart of the valve.

$$\varphi(\sigma,\sigma_*)=\begin{cases}\sqrt{1-(\frac{\sigma-\sigma_*}{1-\sigma_*})^2} & \sigma\geqslant\sigma_*,\\ 1 & \sigma<\sigma_*,\end{cases} \tag{11}$$

where p_s is the supply pressure, p_a the local atmosphere pressure, A_{u1} and A_{d1} the charging effective section area of the two valves, A_{u2} and A_{d2} the discharging effective section area of the two valves, T_s the supply air temperature, T_u and T_d the temperatures of the two chambers, c negotiability of the valve, R the molar gas constant, and σ_* the ratio of critical pressure.

Adiabatic processes in the two chambers are assumed, and the temperatures of the two chambers are supposed all equal to the supply air. Thus, the pressure dynamic equations in each chamber can be written as

$$\dot{p}_u=nRT_s\frac{q_u}{V_u}-n\frac{\dot{V}_u p_u}{V_u}=nRT\frac{\psi_{u1}(p_u,p_s)A_{u1}-\psi_{u2}(p_u)A_{u2}}{V_u}-n\frac{\dot{V}_u p_u}{V_u}, \tag{12}$$

$$\dot{p}_d=nRT_s\frac{q_d}{V_d}+n\frac{\dot{V}_d p_d}{V_d}=nRT_s\frac{\psi_{d1}(p_d,p_s)A_{d1}-\psi_{d2}(p_d)A_{d2}}{V_d}+n\frac{\dot{V}_d p_d}{V_d}, \tag{13}$$

where n is the thermal coefficient and V_u and V_d the volumes of the upper and low chamber, respectively. Owing to the nonlinearity between the pressure and the effective section area, it is difficult to obtain a linear model from Eqs. (12) and (13). In this part of the report, a linear model around the work point is built by linearization method.

If (u_0,p_0) is a work point, Eq. (12) is linearized around the point (u_0,p_0) by

$$\begin{aligned}\tilde{q}_u&=\left.\frac{\partial q_u}{\partial A_{u1}}\right|_{p_u=p_0}A_{u1}+\left.\frac{\partial q_u}{\partial A_{u2}}\right|_{p_u=p_0}A_{u2}+\left.\frac{\partial q_u}{\partial p_u}\right|_{p_u=p_0,A_{u10},A_{u20}}p_u\\&=g_1A_{u1}+g_2A_{u2}+f_1p_u,\end{aligned} \tag{14}$$

where A_{u10} and A_{u20} are effective section areas of the valve at $u=u_0$. On condition that effective section areas of the valve is small and system is working near the work point, the relationship between the effective section areas and the control voltage can be approximately considered as linear, namely $A_{u1}=a_1u$ and $A_{u2}=a_2u$. Then by substituting Eq. (14) into Eq. (12), a model of upper chamber around the work point is obtained as

$$\dot{p}_u=\frac{k_{u1}}{V_u}u+\frac{k_{u2}}{V_u}p_u-n\frac{\dot{V}_u p_u}{V_u}, \tag{15}$$

where

$$k_{u1}=nRT_s(g_1a_1+g_2a_2),\quad k_{u2}=nRT_sf_1.$$

By the similar procedure, the model of the low chamber is also obtained, which is

$$\dot{p}_d = \frac{k_{d1}}{V_d}u + \frac{k_{d2}}{V_d}p_d - n\frac{\dot{V}_d p_d}{V_d}. \tag{16}$$

Now supposing the volumes of the chambers are invariant, namely $\dot{V}_u = 0$, $\dot{V}_d = 0$, then the Laplace form of models (15) and (16) are

$$G_u = \frac{R_1}{1+T_1 s}, \quad R_1 = -\frac{k_{u1}}{k_{u2}}, \quad T_1 = -\frac{V_u}{k_{u2}}, \tag{17}$$

$$G_d = \frac{R_2}{1+T_2 s}, \quad R_2 = -\frac{k_{d1}}{k_{d2}}, \quad T_2 = -\frac{V_d}{k_{d2}}. \tag{18}$$

These models are equivalent to a first-order inertia system. In addition, the influence of volume changing will be considered by velocity compensation in the control system structure, it will be introduced in Section 5.4.

4.2. Controller design

Based on the above model, predictive control algorithm is used for the controller design. Several types of models such as step-response model, impulse-response model and state-space model can be used in MPC. Contrast to other models, the state-space representation can provide a unique insight into system properties, improve the system performance and simplify the analysis. In this paper, the predictive controller based on the state-space form is designed for pressure tracking control.

The discrete time state space model of a plant with *nu* inputs and *ny* outputs is

$$x(k+1) = Ax(k) + Bu(k), \quad y(k) = Cx(k), \tag{19}$$

where $x \in R^n$, $u \in R^{nu}$, and $y \in R^{ny}$.

Define the input and predictive output horizon vectors at k instant as

$$U(k) = [\,\hat{u}(k|k) \quad \cdots \quad \hat{u}(k+i|k) \quad \cdots \quad \hat{u}(k+H_u-1|k)\,]^{\mathrm{T}}, \quad i = 0,\ldots,H_u-1, \tag{20}$$

$$Y_p(k) = [\,\hat{y}(k+1|k) \quad \cdots \quad \hat{y}(k+i|k) \quad \cdots \quad \hat{y}(k+H_p|k)\,]^{\mathrm{T}}, \quad i = 1,\ldots,H_p. \tag{21}$$

The task of prediction is to predict output $\hat{y}(k+i|k)$ up to H_p step ahead and give projected input $\hat{u}(k+i|k)$ for H_u ahead. The integer H_p and H_u are the length of the output horizon and input horizon, respectively, usually $H_u \leqslant H_p$ and $H_p \geqslant 1$.

The input-increment sequence $\Delta U(k)$ is given by

$$\Delta U(k) = [\,\Delta\hat{u}(k|k) \quad \cdots \quad \Delta\hat{u}(k+i|k) \quad \cdots \quad \Delta\hat{u}(k+H_u-1|k)\,]^{\mathrm{T}}, \quad i = 0,\ldots,H_u-1. \tag{22}$$

So the component of the input sequence $U(k)$ can be written as

$$\hat{u}(k+i|k) = \Delta\hat{u}(k+i|k) + \cdots + \Delta\hat{u}(k|k) + u(k-1), \quad i = 0,\ldots,H_u-1, \tag{23}$$

here $u(k-1) = \hat{u}(k-1|k-1)$, namely the actual input to the plant at $k-1$ instant.

By iterating the plant model (19), the predictive output sequence can be obtained as

$$\begin{aligned}\hat{y}(k+i|k) = {} & CA^i x(k) + C(A^{i-1} + \cdots + A + I)B\Delta\hat{u}(k|k) + \cdots + CB\Delta\hat{u}(k+i-1|k) \\ & + C(A^{i-1} + \cdots + A + I)Bu(k-1), \quad i = 1,\ldots,H_u,\end{aligned}$$

$$\begin{aligned}\hat{y}(k+i|k) = {} & CA^i x(k) + C(A^{i-1} + \cdots + A + I)B\Delta\hat{u}(k|k) + \cdots + C(A^{i-H_u} + \cdots + A + I)B\Delta\hat{u}(k+H_u-1|k) \\ & + C(A^{i-1} + \cdots + A + I)Bu(k-1), \quad i = H_u+1,\ldots,H_p.\end{aligned} \tag{24}$$

Then $Y_p(k)$ can be expressed as

$$Y_p(k) = \Psi x(k) + \Upsilon u(k-1) + \Theta\Delta U(k), \tag{25}$$

here $\Psi = C[A \quad \cdots \quad A^{H_p}]^{\mathrm{T}}$, $\Upsilon = C\left[B \quad \cdots \quad \sum_{i=0}^{H_p-1} A^i B\right]^{\mathrm{T}}$, and Θ is a Markovian matrix

$$\Theta = C\begin{bmatrix} B & \cdots & 0 \\ AB+B & \cdots & 0 \\ \vdots & \ddots & \vdots \\ \sum_{i=0}^{H_u-1} A^i B & \cdots & B \\ \sum_{i=0}^{H_u} A^i & \cdots & AB+B \\ \vdots & \vdots & \vdots \\ \sum_{i=0}^{H_P-1} A^i B & \cdots & \sum_{i=0}^{H_P-H_u} A^i B \end{bmatrix}_{H_p \times H_u}. \tag{26}$$

Now $Y_p(k)$ can be further written as

$$Y_p(k) = Y_f(k) + \Theta \Delta U(k). \tag{27}$$

$Y_f(k) = \Psi x(k) + \Upsilon u(k-1)$ is the free response when $\Delta U(k) = 0$. In Eq. (27), only $\Delta U(k)$ is unknown and can be obtained by solving the objective function.

The goal of the controller is to let $Y(k)$ follow the setpoint $\Gamma(k)$. The tracking error is defined as $E(k) = \Gamma(k) - Y_p(k)$ and is to be minimized for a bounded input. This is accomplished by minimizing the following performance index

$$J = (\Gamma(k) - Y_p(k))^{\mathrm{T}} Q(\Gamma(k) - Y_p(k)) + \Delta U(k)^{\mathrm{T}} R \Delta U(k). \tag{28}$$

Define $\varepsilon(k) = \Gamma(k) - Y_p(k)$ as the predicted output error, then

$$\begin{aligned} &\frac{\partial J}{\partial \Delta U} = 2\Theta^{\mathrm{T}} Q(\Theta \Delta U(k) - \varepsilon(k)) + 2R\Delta U(k) = 0, \\ &\Delta U(k) = K(\Gamma(k) - Y_f(k)) = K\varepsilon(k), \end{aligned} \tag{29}$$

where

$$K = (\Theta^{\mathrm{T}} Q \Theta + R)^{-1} \Theta^{\mathrm{T}} Q. \tag{30}$$

The control increment sequence $\Delta U(k)$ covers the whole input horizon H_u, but only the part of the solution corresponding to the first step is used. So define k_m as the first row of the K:

$$k_m = eK, \quad e = [I_{mu} \quad 0 \quad \cdots \quad 0]. \tag{31}$$

Then the control increment and the control input at the instant k are

$$\Delta u(k) = \Delta \hat{u}(k|k) = k_m(\Gamma(k) - Y_f(k)) = k_m \varepsilon(k), \tag{32}$$

$$\begin{aligned} u(k) &= u(k-1) + \Delta u(k) = u(k-1) + k_m(\Gamma(k) - Y_f(k)) \\ &= k_m \Gamma(k) - k_m \Psi x(k) + (1 - k_m \Upsilon) u(k-1). \end{aligned} \tag{33}$$

Thus, the command $u(k)$ depend on the previous input horizon $U(k-1)$, on the actual state $x(k)$, and on the control command $\Gamma(k)$ up to H_p steps ahead. The block diagram for the close loop system is presented in Fig. 6.

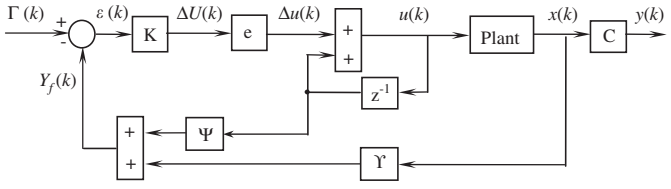

Fig. 6. Close loop system block diagram of MPC.

5. Experiment study

To demonstrate the capability of predictive controller, an experiment system of the inner loop is implemented first. The MPC controller is implemented using the real time control system composed of PXI-8176 controller and PXI6070E data acquisition card of NI company. Program is written with LabVIEW RT.

In the experiment, the pressure work point is set at 4.4 kgf/cm^2. According to Section 4.1, a linearized pneumatic model of the upper chamber at this work point is

$$G(S) = \frac{2.22}{1 + 0.7191S}. \tag{34}$$

Then converting Eq. (34) to the state space form

$$x(k+1) = Ax(k) + Bu(k), \quad y(k) = Cx(k), \tag{35}$$

where $x(k) = p(k)$, $A = [-1.39]$, $B = [3.09]$, $C = [1]$. This model is a first-order system and there is a steady output error if a conventional proportion controller is used. In MPC, the increment input form is used for realizing no steady error tracking.

In the following part of the section, performances of the pressure control system will be studied from different aspects.

5.1. Control parameter choice

In MPC, there are four control parameters, i.e. Q and R, H_p and H_u, that should be defined.

The weighting matrices R and Q are the tuning parameters of the optimal design, and their choice will significantly influence performance and stability of the system. A diagonal matrix $R = \rho I$ has been chosen as the control weighting matrix, where $\rho > 0$ is a scalar. The tracking error weighting matrix Q has the structure defined by Eq. (36):

$$Q = \mathrm{diag}(q, \alpha q, \ldots, \alpha^{H_p - 1} q). \tag{36}$$

The scalar α is called forgetting factor. The most recent output is given a unit weight, and the future output penalized exponentially. With this arrangement, the choice of R and Q is reduced to the choice of parameters ρ, α and q.

In the real experiment system, weighting matrices R and Q are such chosen that the output error is small while the control effort is maintained within reasonable limits. For a diagonal control weighting matrix $R = \rho I$, the parameter $\rho = 1$ is chosen as 1. Weighting matrix Q is defined by Eq. (36), in which $q = 1.5$. Coefficient α^{k-1} in the weighting matrix is the weight of the kth error component in the output horizon. Simulations have been performed for determining the value of parameter α. The plot of the Euclidean norm of tracking error $||y - y_0||_2$ versus α is shown in Fig. 7 for different lengths of the predictive horizon. Here $H_u = 3$. Fig. 8 plots the value of α for which the tracking error is minimal. Fig. 8 shows that a longer predictive horizon generates a smaller forgetting factor.

In the experiment, pressure tracking control with different H_p and α is performed using the real time control system. Fig. 9 presents curves of pressure response versus H_p. The values of other control parameters are set, respectively, as $H_u = 3$, $\rho = 1$ and $\alpha = 2$. As shown in the figure, with an increment of H_p from 12 to 16, overshoot of the response is decreased 1.2% and the stability of close loop is improved, but the adjustment time of the response is also increased accordingly. Fig. 10 plots the pressure response versus α. Two curves in this figure are corresponding to $\alpha = 1.5$ and 2.1, respectively. The dynamic performance of the system can be improved by adding the forgetting factor α.

5.2. Command horizon generator

In every instant k of MPC, the input command within future H_p needs to be given. So a command horizon generator is built in order to provide input command within future H_p horizon. The state-space representation

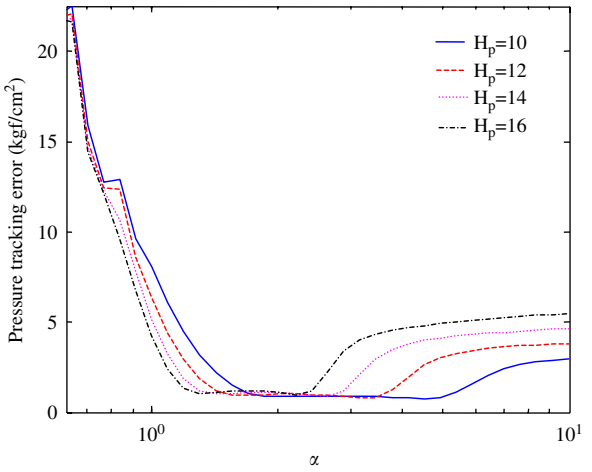

Fig. 7. Pressure tracking error curves versus α.

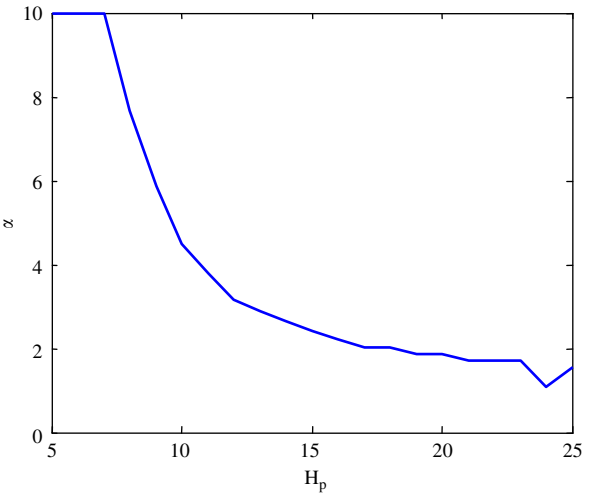

Fig. 8. α versus H_p for minimal tacking error.

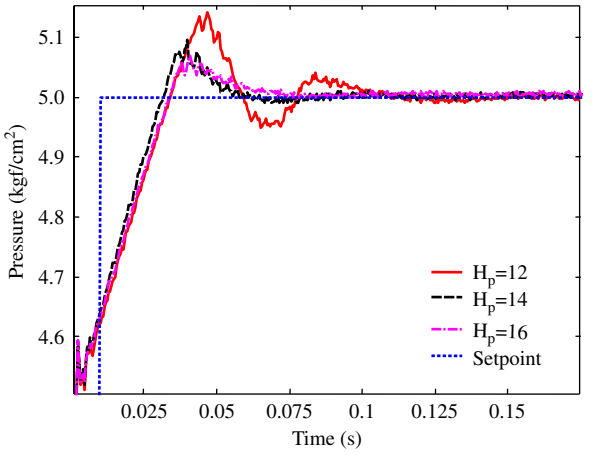

Fig. 9. Pressure responses versus H_p.

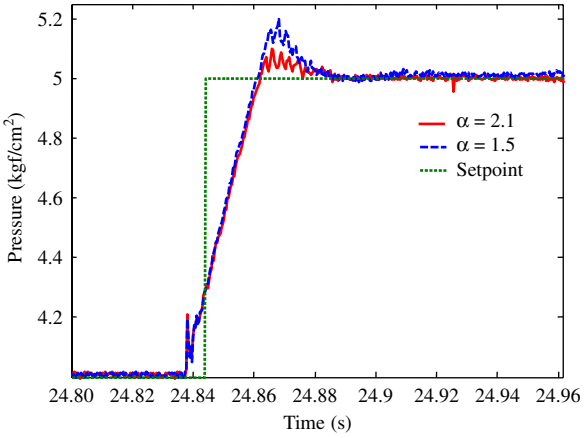

Fig. 10. Pressure responses versus α.

of the command horizon generator is

$$x(k+1) = A_r x(k) + B_r u(k),$$
$$y(k) = C_r x(k) + D_r u(k), \tag{37}$$

where $x(k) = [\,r(k+1|k) \quad \cdots \quad r(k+i|k) \quad \cdots \quad r(k+H_p-1|k)\,]^{\mathrm{T}}$, $u(k) = [r(k+H_p|k)]$, A_r, B_r, C_r and D_r are, respectively:

$$A_r = \begin{bmatrix} 0 & I & 0 & \cdots & 0 \\ 0 & 0 & I & \cdots & 0 \\ & & \cdots & & \\ 0 & 0 & 0 & 0 & I \\ 0 & 0 & 0 & 0 & 0 \end{bmatrix}_{H_p-1 \times H_p-1}, \quad B_r = \begin{bmatrix} 0 \\ 0 \\ \vdots \\ 0 \\ I \end{bmatrix}_{H_p-1 \times 1},$$

$$C_r = \begin{bmatrix} I & 0 & \cdots & 0 \\ 0 & I & \cdots & 0 \\ & \cdots & & \\ 0 & 0 & \cdots & I \\ 0 & 0 & \cdots & 0 \end{bmatrix}_{H_p \times H_p-1}, \quad D_r = \begin{bmatrix} 0 \\ 0 \\ \vdots \\ 0 \\ I \end{bmatrix}_{H_p \times 1}.$$

The structure of the command horizon generator is showed in Fig. 11.

5.3. Model error correction

The work point model achieved in Section 4.1 is impossible to be identical with the real plant due to such factors as nonlinearity, time delay and so on. However, MPC requires that the output of a model should be equal to the real output, otherwise it will produce a steady error. To eliminate this steady error, as showed in Fig. 12, a feedback correction item using the difference between the real output and the model output was added.

As shown in Fig. 12, the free response $Y_f(k)$ is changed to $Y'_f(k)$, and

$$Y'_f(k) = \Psi x(k) + \Upsilon u(k-1) + H(y(k) - y_m(k)), \tag{38}$$

where H is the gain of error correction. The predictive output now becomes

$$Y_p(k) = Y'_f(k) + \Theta \Delta U(k). \tag{39}$$

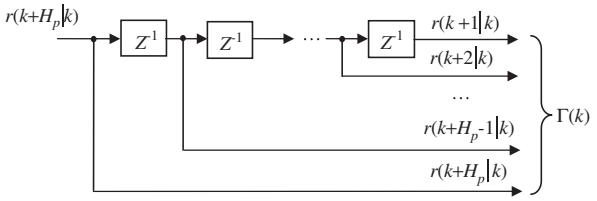

Fig. 11. Command horizon generator.

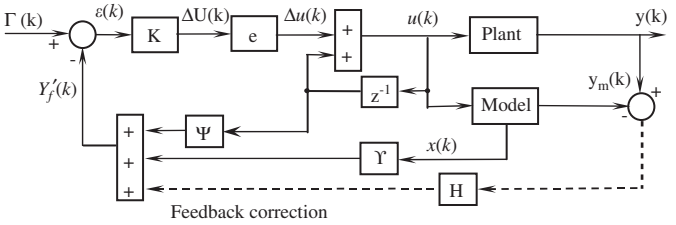

Fig. 12. Predictive controller system with feedback modification.

Put Eq. (38) into Eq. (33), it is obtained that

$$u(k) = u(k-1) + k(\Gamma(k) - Y'_f(k)) = k\Gamma(k) - k\Psi x(k) + (1 - k\Upsilon)u(k-1) - kH(y(k) - y_m(k)). \quad (40)$$

At the steady state of the system,

$$\Delta U_\infty(k) = 0 \quad \text{namely } u_\infty(k) = u_\infty(k-1), \quad (41)$$

$$y_{m\infty}(k) = y_{f\infty}(k) = \Psi x(k) + \Upsilon u(k-1) \quad (42)$$

and thus Eq. (40) can be simplified as

$$0 = \Gamma(k) - \Psi x(k) - \Upsilon u(k-1) - Hy_{m\infty}(k) - Hy_\infty(k). \quad (43)$$

When $H = 1$,

$$\Gamma(k) = y_\infty(k). \quad (44)$$

By adding the feedback correction, it improves the robustness of model mismatch and realizes no steady error tracking. Fig. 13 is the experiment results. As shown, with the feedback correction item, the steady error is reduced effectively.

5.4. Velocity compensation

In Section 4.1, the work point model is obtained on condition that the volume of the chamber is constant. But during the operation, due to the motion of the piston, volumes of the upper and low chambers will change continuously. Therefore, in Eq. (15) and (16), the differential component $n(\dot{V}_u p_u / V_u)$ will affect the pressure change to some degree.

It can be seen from Eq. (15) and (16) that the derivative of pressure is not only decided by the flux but also the relative velocity of the piston. Because the achieved model is around the work point, $n(p_u/V_u)$ can be approximately taken as a constant. To cope with the effect of volume variation, velocity compensation is added to the control structure (Fig. 14). In the figure, the adding feedback is made up of relative velocity between the piston and base.

Fig. 15 shows the experiment results of upper and low chamber pressure response when the piston moves.

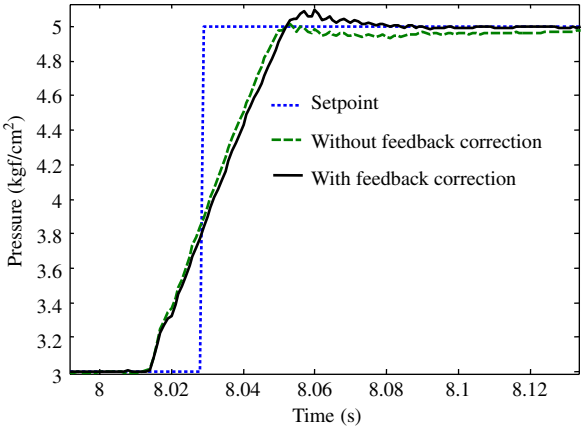

Fig. 13. Feedback modification control.

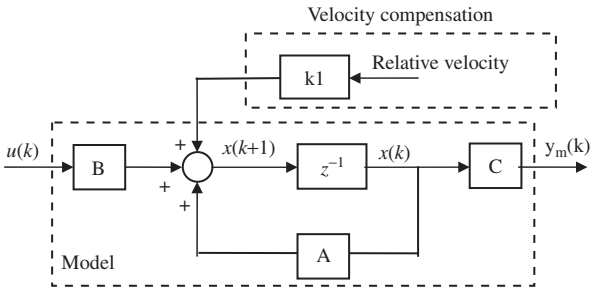

Fig. 14. Pressure control with velocity compensatory.

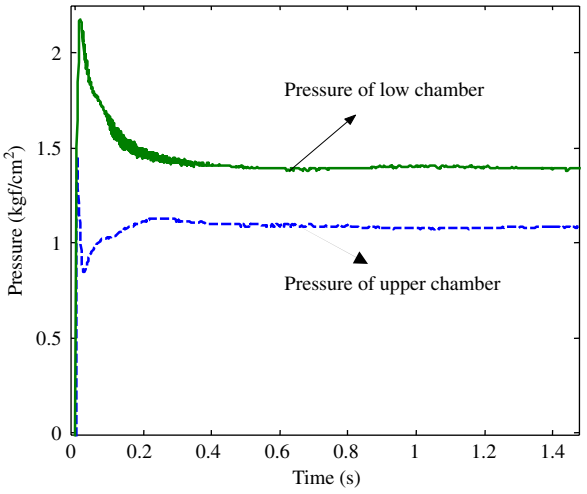

Fig. 15. Pressure responses of upper and low chamber.

6. Conclusion

According to the particular environment of the launch vehicle and characteristics of most widely studied and applied actuators, and the energy source availability of the launch vehicle, the actuator with pneumatic control is chosen to be the element for the construction of an active vibration isolation platform for the

whole-spacecraft vibration isolation. Nevertheless, applications of pneumatic actuators also bring about some problems that include low reaction speed and narrow frequency band. To ensure the performance of the active control system, a cascade control with double close loop structure is proposed. Among this control structure, the inner loop is the pressure control based on the MPC and the outer loop is the isolation control with velocity feedback.

By introducing a predictive control algorithm based on the state space representation and adding functions of model error correction and velocity compensation to the controller structure, problems associated with the pressure tracking control are successfully solved. Experiment results have proven the suitability of the proposed pressure tracking control system for ensuring the performance of the active vibration isolation control system.

References

[1] D. Sciulli, E. Fosness, A. Das, Soft ride for satellites, *Engineering, Construction and Operations in Space (Space 98)*, April 26–30, 1998, pp. 94–101.

[2] P. Wilke, C. Johnson, P. Grosserode, Whole-spacecraft vibration isolation for broadband attenuation, *Aerospace Conference Proceeding*, IEEE, New York, April 2000, pp. 315–321.

[3] K.K. Denoyer, C.D. Johnson, Recent achievements in vibration isolation systems for space launch and on-orbit applications, *AIAA Space 2001—Conference and Exposition*, Albuquerque, NM, August 28–30, 2001, pp. 1–11.

[4] C.D. Johnson, P.S. Wilke, K.R. Darling, Multi-axis whole-spacecraft vibration isolation for small launch vehicles, *SPIE Conference on Smart Structures and Materials*, Newport Beach, CA, March 4–8, 2001, pp. 4331–4340.

[5] P.S. Wilke, C.D. Johnson, Payload isolation system for launch vehicles, *Proceedings of SPIE. Smart Structures and Materials—Passive Damping and Isolation*, 1997, pp. 20–30.

[6] D.L. Edberg, C.D. Johnson, L.P. Davis, E.R. Fosness, On the development of a launch vibration isolation system, *Proceedings of the SPIE Smart Structures Conference*, San Diego, CA, 3–6 March 1997, pp. 31–37.

[7] D.L. Edberg, B. Bruce, G. James, W. Pau, D. Torey, Passive and active launch vibration studies in the LVIS program, *Proceedings of SPIE—The International Society for Optical Engineering v 3327*, March 18–20, 1998, pp. 411–422.

[8] K. Farshad, R. Jahangir, E.R. Scott, Three degrees-of-freedom adaptive-passive isolator for launch vehicle payloads, *The International Society for Optical Engineering* 3991 (2000) 164–175.

[9] D. Thayer, J. Vagners, A. von Flotow, C. Hardham, K. Scribner, Six-axis vibration isolation system using soft actuators and multiple sensors, *Journal of Spacecraft and Rocket* 39 (2) (2002) 206–212.

[10] J.M. Maciejowski, *Predictive Control with Constrains*, Biddles Ltd., Guildford and King's Lynn, Great Britain, 2002 (pp. 81–88).